AEROFOIL SELECTION AND SPANWISE PLACEMENT IN AERODYNAMIC DESIGN AND OPTIMIZATION OF TILTROTOR BLADES

Antonio Pagano, a.pagano@cira.it, CIRA, Italian Aerospace Research Centre (Italy)

The aim of this paper is to investigate the influence of the aerofoil sections and their distribution along a tiltrotor blade on the rotor aerodynamic performance. Several numerical tools are linked into code networks by means of a software environment for code integration and optimization to automatically perform such investigations. The developed methodology is applied on a realistic configuration based on the ADYN European tiltrotor blade geometry. Two sets of five aerofoils with decreasing values of the thickness-to-chord ratio are used. It is demonstrated that the present methodology can be successfully adopted both in the design and optimization of tiltrotor blades. Thinning the baseline blades by replacing the thicker aerofoils with the optimum distribution of the other remaining aerofoils over the blade span is found to be a suitable way to improve the tiltrotor performance at the nominal working conditions. The present methodology can also give useful insights for the assessment of new rotor concepts such as variable speed or variable span rotors where the aerofoils are expected to play an even greater role.

1. INTRODUCTION

Tiltrotors use the rotors both in helicopter and airplane mode. By limiting the analysis to axial flight, blade aerofoils experience different flow conditions when the rotor operates as a helicopter rotor or as a propeller. In the blade design process aerofoils are selected and placed along the span not only on the basis of their aerodynamic performance (mainly, *L/D*, $C_{l_{max}}$, M_{dd}) but also in coherence with the structural requirements (blade robustness and margin of safety). In this regard, thickness-to-chord ratio (*t/c*) is a significant parameter because of its impact over both the aforementioned aerodynamic aerofoil properties and the structural aspects. Despite aerofoil selection and placement have a remarkable impact on tiltrotor aerodynamic performance, very little literature exists on this subject.

Romander[1] investigated by means of Navier-Stokes CFD analyses the influence of the aerofoil thickness on the rotor performance in airplane mode by thinning alternatively only the inboard cross section (influencing the blade shape up to 50% of the span) or the whole blade. He found that scaling down the aerofoil thickness over the entire blade gave more benefits than scaling the root section only. Rotor comprehensive calculations by Acree et al.[2] confirmed that a thinner inboard section was beneficial for cruise propulsive efficiency allowing for a reduced performance gain in hover as well. They also emphasized that the addition of aerofoils related parameters to the design variables made a blade shape optimization almost impractical because of the significant size of the design space. Stahlhut & Leishman[3] optimized the thickness-to-chord ratio spanwise distribution by representing the properties ($C_{l_{max}}$ and M_{dd}) of next generation aerofoils as functions of *t/c* by using an improved BEMT (Blade Element Momentum Theory) model. They observed that a baseline tiltrotor blade with a 0.12 spanwise constant value of *t/c* performed better when equipped with thicker inboard sections (maximizing hover performance) and thinner outboard sections (maximizing propeller efficiency).

2. GOALS

The main purpose of the present paper is to contribute to this specific subject by addressing the blade design and optimization task with particular reference to the following aspects: influence of the thickness distribution (inboard section thickness, length of blade segments with constant aerofoil thickness and length of blade segments whose internal sections are obtained by interpolating the external aerofoil geometries), impact of different aerofoil families and their nonlinear spanwise placement.

This kind of investigation assumes today an ever increasing relevance since the rotorcraft community is debating on the effectiveness of some technologies aiming at rotor performance improvements. Technologies allowing variable span rotors and variable angular velocity rotors, applied both separately and simultaneously, have become more and more popular and explored by mono/multi-disciplinary approaches. For these advanced configurations, aerofoil selection and position may play a very critical role: in fact, individual aerofoils may undergo different flow characteristics depending on the actual peripheral speed they are exposed to. The sectional peripheral speed may vary either when the distance of the blade section from the hub centre is altered (elongable/retractable rotor) or when the angular velocity changes (variable speed rotor). The combination of the two technologies adds even more working conditions for aerofoils so that the task of their selection and placement is very complicated.

Without entering the technical feasibility and the discussions associated with structure, weight, power and vibration challenges of these technologies, the paper intends to explore the aerodynamic potential benefits expected by a careful aerofoil selection and placement. As a complement of early investigations on planform shapes,[4] CIRA presents the outcome of a study about the aerofoils choice and positioning effects on proprotor aerodynamic performance (hover figure of merit and propeller aerodynamic efficiency) by taking simultaneously into account many of the influencing blade constructive parameters, including aerofoil shape and spanwise position, either for conventional proprotors and for rotors with variable blade span, continuous variable angular velocity and concomitant variable span and angular velocity.

Investigations exploit the predictions of a very flexible in-house software performance code which allows to separately manage planform parameters (spanwise distribution of chord, built-in twist, leading-edge line, sweep and dihedral angles) and aerofoil related details (number of distinct aerofoils equipping the blade, spanwise aerofoil position, blade segment with constant or interpolated sections, kind of aerofoil geometry and look-up table availability).

3. OUTLINE OF METHODS

The methodology presented in this work completes and improves the one described in [4] which the reader can refer to for a more exhaustive description of the software tools necessary to arrange a shape optimization procedure. In this section only the tools involved in the investigations are recalled; those showing little enhancements are summarized whereas more details are given when major modifications are introduced. It is anticipated that among the Multidisciplinary Design Analyses (MDA) those based on CFD coupling procedures are not used here. Automatic volume grid generation, CFD codes and coupling procedures are thus not outlined.

3.1. The integration and optimization environment

The process integration and optimization tool OPTIMUS® from Noesis Solutions[5] is the frontend to integrate arbitrary analysis codes, to automate the process execution, to control data exchange, to split the process over a heterogeneous computational environment where analysis codes run on different computer platforms, and to post-process results. The key functionalities of optimization methods are fully exploited in order to address the search of global optima. DOE (Design Of Experiments), RSM (Response Surface Methodology), Gradient/Genetic based algorithms are, respectively, available for the exploration of the design space, the approximation of models, the design optimization. Optimus 10.10 is the version of this software package used for all of the applications herein shown.

3.2. Blade surface parameterization

A critical step in the automated design optimization process is the selection of an efficient way to parametrically describe the geometry. The general aim is to reduce the number of design variables while retaining the ability to capture a global range of designs. Before the emergence of the CAD surface representation, a helicopter rotor blade was generated by positioning, rotating and scaling 2D aerofoils (in non-dimensional coordinates) along the blade span. The approach followed here to parameterize the blade geometry retrieves the traditional approach to design the blade, thus, the planform shape is separated by the sectional shape. This means that the blade shape is modified by means of constructive parameters affecting the blade planform whereas the sectional shape is modified by selecting the appropriate set of aerofoils and by distributing them along the blade span.

In order to perturb the design surface in a continuous way, six constructive parameters are identified for each spanwise station: chord length, geometric twist, vertical and horizontal leading edge offset, sectional sweep and dihedral angles. Under the hypothesis of parallel planar sections, these parameters reduce to the first four. For simple blade shapes (e.g., rectangular shape), the constructive parameters at the inner and outer stations can be used. Nevertheless, the number of spanwise stations is expected to increase especially for complex blade shapes and highly nonlinear parameter variations. Of course, the number of sections needs to be limited anyway otherwise the number of design variables becomes larger and larger. For this reason, the adopted parametric model is based on three or, at most, on four control sections. Generally the first and the last section correspond to the sections limiting the geometry to be optimized. On the contrary, the intermediate control sections are chosen by the user. Indeed, the user chooses the position of the intermediate control sections and a software tool calculates the constructive parameters by interpolating on the closest spanwise stations. Usually the number of the blade spanwise stations are greater than the number of the control stations. Thus, to appropriately characterize the blade, the constructive parameters associated to the spanwise sections in excess are not considered as design variables but they are modified according to predefined interpolation functions which distribute the deltas of the surrounding design variables.

As far as the sectional shape is concerned, two more design variables are introduced. The first one modifies the length of the blade segments, which the blade is subdivided into, with the aim to differently distribute the aerofoils. The second one identifies the set of aerofoils which equip the blade.

On the basis of what has been discussed above, a geometry blade shape modeler, PRE_GEOM, has been developed and embedded in the optimization processes. Indeed, the blade shape module can also deal with the variation of the blade angular velocity (expressed in terms of RPM) and the blade rotor radius. These quantities are linked together because of the definition of blade tip speed which has a significant impact on the aerodynamic conditions. When the blade radius varies, three options are available (see Figure 1): the length of each blade segments is proportionally modified according to the radius length, the blade is rigidly shifted forward, the blade tip radially extends (telescopic blade).

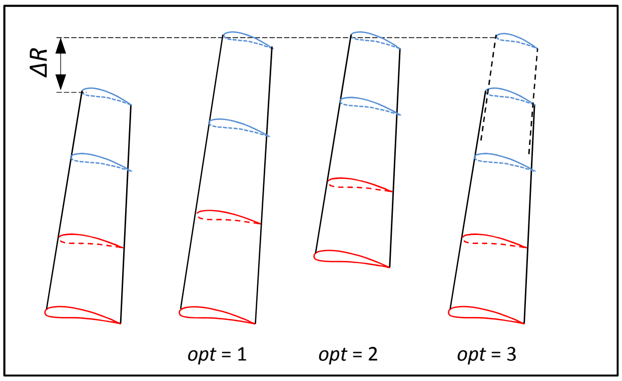

Figure 1: options for varying the rotor radius.

The latter two cases imply limitations on the root section and on the twist distribution.

In conclusion, the parameterization module reads the initial geometry and computes for each section the new sectional constructive parameters according to the current set of the design variables. The output of this module is the input file for generating a new surface grid. If the blade is modified by means of three control sections, the global number of design variables for a full parameterization is 4×3+8=20 (respectively, chord, twist, horizontal and vertical leading edge offset for three sections, the position of the intermediate section, the interpolating function, a variable for the blade segment length, a variable for the aerofoil set, the RPM value, the rotor radius, the percentage of the actual radius by which the blade may be elongated and a variable for choosing the elongable/retractable strategy).

3.3. Blade surface generator

The blade geometry is constructed by using two separate kinds of input data, the planform data and the aerofoil data. The file including the planform data contains chord, leading edge line offset, position around which the twist is implemented and the angles to rotate the aerofoil around the three axes for a given number of radial stations. The file of the aerofoil data specifies the aerofoil name, the path where the file with the non-dimensional coordinates of the aerofoil can be found, the radial position where it is mounted and the path where the relative look-up tables are stored, if available. After the aerofoils are read, they are positioned along the blade span and shaped according to the planform data.

3.4. Aerofoil selection and spanwise distribution module

The file with aerofoil input data contains all of the available aerofoils equipping the reference blade. This file can be edited to add or delete aerofoils. Starting from it, a module selects the aerofoils with different geometries and generates as many aerofoil input data as the possible combinations of aerofoils which are distributed over the span with the only constrain of a thickness-to-chord ratio decreasing from blade root to tip.

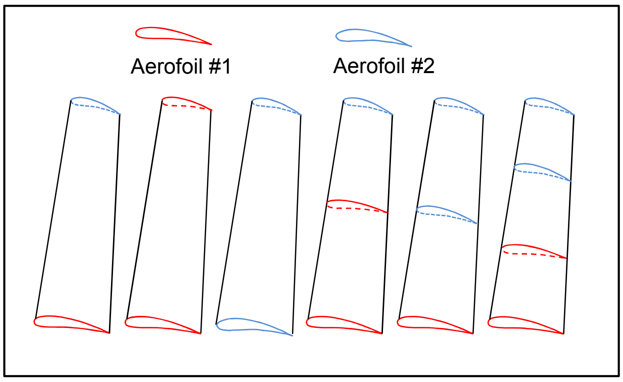

Figure 2: possible blade segmentations with two different aerofoils.

Indeed the blade is initially divided into constant-length radial elements which can be of two kinds, those with an equal aerofoil geometry and those whose geometry is linearly interpolated with the two different aerofoils at the blade segment extremes.

In the simple case of a blade having just two different aerofoil geometries (respectively, at the blade root and tip), this module generates six different blades as depicted in Figure 2. The greater the number of different aerofoils, the greater the number of combinations. All of the blade with different aerofoil combinations are listed, progressively numbered and stored into a file. Furthermore, each blade segment is characterized by an increasing number (starting from the inner one) and by the parameter *len* which is used to stretch or squeeze its radial length. Figure 3 illustrates the effect of the parameter *len* on the radial length of the blade segment 2. A negative value of *len* is used to block the blade element length to its initial value.

3.5. ARTIST

ARTIST (Aerodynamics and Rotor Trim by Implementing Simple Theories) is a numerical code based on the classical blade element momentum theory (BEMT) and provides both the rotor trim and the performance evaluation.

For a rotor with a radius R, whose axial and rotational velocities are respectively V_c and Ω, a blade annulus at a distance y from the centre produces an inflow angle given by

$$\alpha_i = \frac{1}{2\cos\delta}\left[-\left(\sin\delta + \frac{\sigma C_{l_\alpha}}{8rF}\right) + \sqrt{\left(\sin\delta + \frac{\sigma C_{l_\alpha}}{8rF}\right)^2 + \frac{\sigma C_{l_\alpha}}{2rF}(\vartheta + \delta)\cos\delta}\right]$$

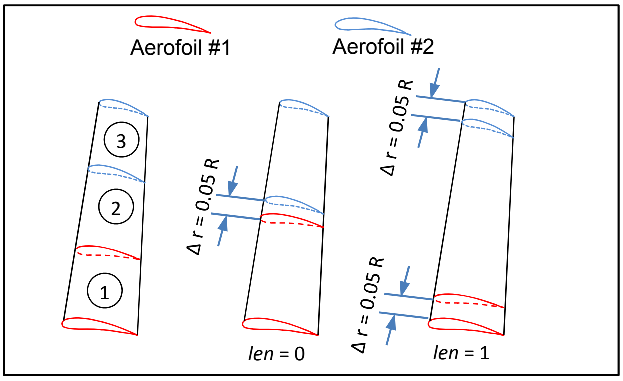

Figure 3: control of the blade segment length. Δr=0.05 R is the minimum blade segment length.

where C_{l_α} is the lift slope, σ is the rotor solidity, F the Prandtl's tip loss factor, ϑ the geometrical incidence introduced by the collective pitch and the local twist, $r = y/R$ and $\delta = \tan^{-1}(V_c/\Omega y)$.

The elementary thrust (dT) and power (dP) are obtained as

$$dT = dL\ \cos(\delta + \alpha_i) - dD\,\sin(\delta + \alpha_i)$$

$$dP = [dL\ \cos(\delta + \alpha_i) - dD\,\sin(\delta + \alpha_i)\,]\Omega y$$

where lift and drag of each blade element are calculated by using the aerodynamic coefficients which are extracted from the look-up tables for axial flights or computed by the Beddoes-Leishman dynamic-stall module for non-axial flights. The elementary thrust and power are integrated over the blade span to compute the rotor thrust and power. Extensive validation on ARTIST has been performed over the past years. Examples concerning axial flights are included in section 5.2 whereas Figures 4 and 5 are relative to 2D and 3D test cases, respectively, where unsteady aerodynamics is involved.

4. THE NUMERICAL PROCESSES

This section is dedicated to the description of the conceptual scheme in which the numerical processes are articulated and to their practical implementation within the OPTIMUS® environment.

4.1. The MDA procedures for tiltrotor performance

CIRA MDA procedures are automatic numerical procedures where software tools are linked together. The software tools typically are analysis codes selected from a simulation library structured on a disciplinary basis (comprehensive rotor codes, CFD codes, grid generators, aeroacoustic codes, … all of them generally offered in multiple versions implementing different mathematical models ranging from simple to very sophisticated ones) and complementary software components (such as code interfaces).

The application of these MDA procedures is documented in several publications[6]-[9] where different optimization problems are addressed: aerodynamic shape optimization for helicopter and turboprop blades aiming at performance maximization, noise reduction, SMA device characterization. The full description of the CIRA MDA procedures is out of the scope of this work. Herein, the simplest MDA procedure is proposed for the aerodynamic analysis of proprotors because of the exploratory nature of this work and because of the large number of simulations expected. It is based on a BEMT performance code already described in section 3.5.

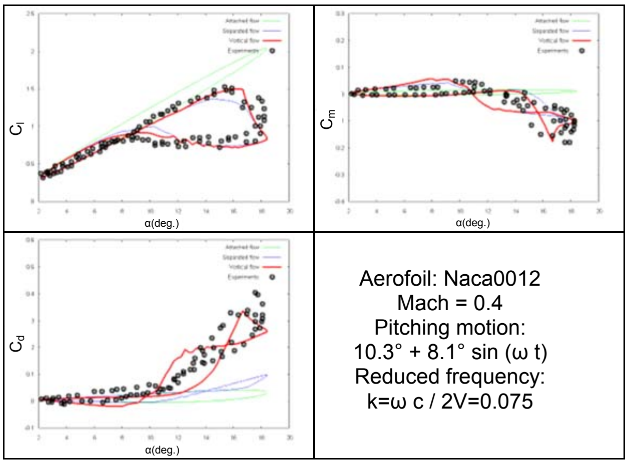

Figure 4: validation of the Beddoes-Leishman model on a pitching aerofoil.

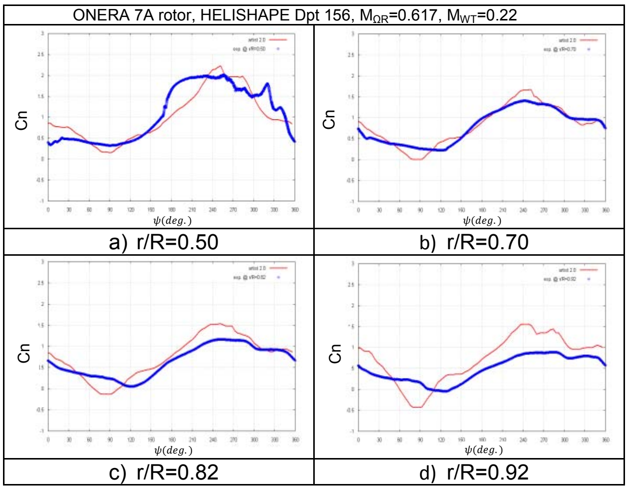

Figure 5: validation of ARTIST on a helicopter rotor in forward flight. Red line=ARTIST; Blue line=Experiments.

4.2. Optimization

The numerical strategy is composed of the following steps:

– the optimization problem is defined by selecting the design space and the objective functions;

– a set of design variables allows to generate a surface geometry and, if CFD is involved, a volume grid too;
– proprotor performance is predicted either by using the stand-alone BEMT code ARTIST or a BEMT-CFD coupling procedure;
– after the evaluation of the objective functions, the optimizer selects a new set of design variables.

Figure 6 offers a snapshot of the OPTIMUS® working area where the analysis task is based on the BEMT-CFD coupling procedure ART-HEL used in [4]. The workflow, once the actual blade surface is generated, is split into two streams in order to predict the rotor performance in helicopter and airplane mode.

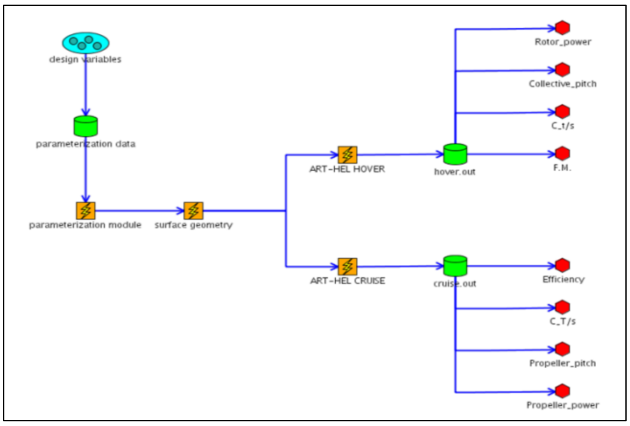

Figure 6: workflow of a CFD-driven optimization process.

In the present study the simpler analysis task based on BEMT is used so that the relative workflow appears as in Figure 7. In this case the workflow aims at calculating the aerodynamic performance of one of the operating conditions meaning that there exists a duplicated workflow for the calculation of the other operating condition.

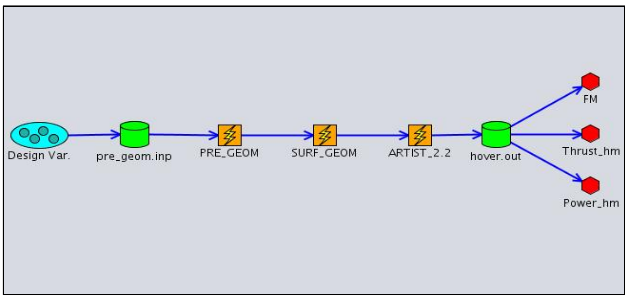

Figure 7: The simple optimization workflow in the OPTIMUS® main window.

This process re-arrangement has a twofold motivation: to better control the angular velocity and rotor radius variations which may be different for the two flight conditions; to fully exploit one of the capability of the optimization environment which is described in the next section.

4.3. Two level processes

Optimus in Optimus® is a tool which allows to perform an optimization on top of another optimization. For the specific problems addressed by this work, it is convenient to have one optimization task on the upper level and two optimization tasks on the inner level. Furthermore, the inner optimizations may be based on different models each of them with its own setting. The design parameters which must have an effect on both the two tiltrotor operating conditions act on the upper level and the parameters which are peculiar to an individual operating conditions act on the inner level. For example, if the aim of the optimization is only to find the optimum distribution of the aerofoils over a frozen blade planform, the upper level will modify the design variables associated with the aerofoils selection and their position along the blade span whereas the inner level will consist on the evaluation of two nominal case (the design variables associated with the planform and with the aerodynamic conditions are not touched). The optimizer selects blades with different aerofoils combinations and modifies the length of the blade segments. When a new blade has been defined in terms of aerofoil data, the lower level of optimization deals with the calculation of the aerodynamic performance. The Optimus in Optimus® process visually appear as in Figure 8.

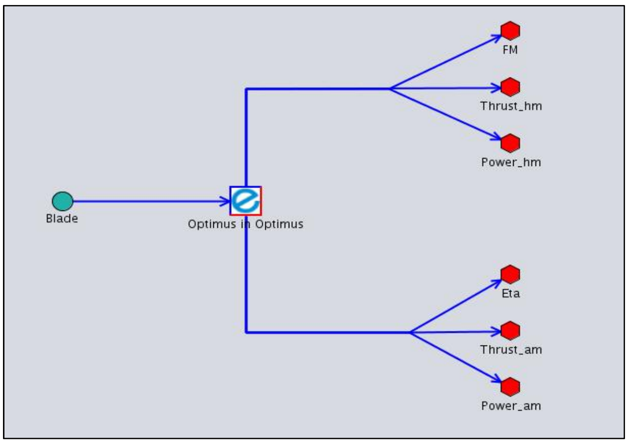

Figure 8: : Optimus in Optimus® workflow.

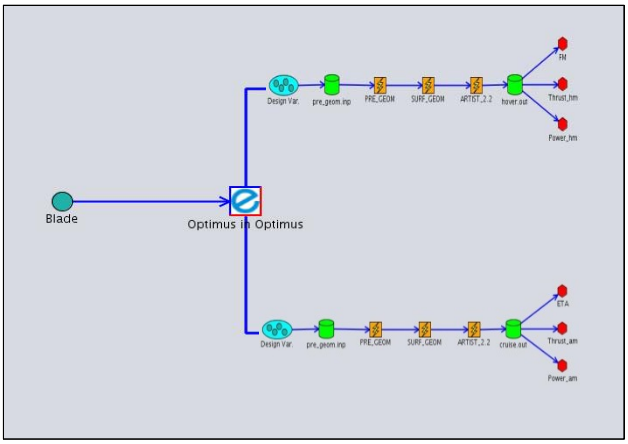

Figure 9: explanation of the Optimus in Optimus® functionality.

Conceptually, it expresses a two level process as depicted in Figure 9 where the upper level optimization drives two inner processes.

It is shown later that this functionality is particularly useful when the problem of morphing blades is approached. If the blade is able to extend by means of a radial rigid movement, chord and twist distributions are, for example, optimized in the upper level. The inner level associated with the helicopter mode acts on the search for the optimum angular velocity and the radius extension. The inner level associated with the airplane mode is only based on the optimum angular velocity search. In the hypothesis of a full morphing blade, it is already possible to perform this two level process: the upper lever once again deals with the aerofoils selection and distribution and the inner level finds the optimum planform shape both for helicopter and airplane mode acting independently on design variables such as chord length, geometric twist, vertical and horizontal leading edge offset, angular velocity and radius extension.

5. DESCRIPTION OF THE CASE STUDY

Within the interrelated CTP (Critical Technology Projects) research projects TILTAERO and ADYN of the 5th FP (Framework Programs) of the European Commission, an articulated experimental campaign[10] was conducted on the ERICA[11] rotor and on its aero-acoustically optimized version, the ADYN rotor. This rotor, described in [12], was subsequently selected to equip a tiltrotor model (full configuration) currently under investigation[16] in the project NICETRIP (6^{th} FP of the European Commission). The ADYN model rotor has a diameter of about 3 m and the blades are characterized by a double sweep angle, with anhedral angle at the tip and a complex non-linear twist and chord span distribution[13]-[15]. Its blade (Figure 10), limited to the aerodynamic part (from r/R=0.25 to the tip) is used for this exercise.

5.1. Setup of the case study

The case study which has been chosen to illustrate the capabilities of the implemented numerical processes is based on the ADYN rotor and it is divided in four subcases each of them addressing a specific optimization problem. Thus, despite the exploratory nature of this work, the ADYN blade shape has been chosen as baseline configuration. Two sets of five aerofoils were circulated during the ADYN project. The performance characteristics of these sets are included in Table 1 and Table 2. All of the subcases share the objective functions: the rotor performance is to be maximized at two nominal aerodynamic conditions: in hover flight, the rotational tip velocity (in terms of Mach number) is $M_{\Omega R}$=0.63 and the thrust coefficient is C_T=0.021; in level flight the rotational tip velocity is $M_{\Omega R}$=0.532, the advance flight velocity is M_{WT}=0.58 (350 Kn at 7500 m) and the rotor load is C_T=0.0157. The length of the blade segments and the aerofoil geometries allocated in there, the twist distribution, the rotor radius, the angular rotation are the main design variables investigated. The blade geometry can be modified in the radial range r/R=[0.25, 1.0] where r and R are, respectively, the local and nominal radius.

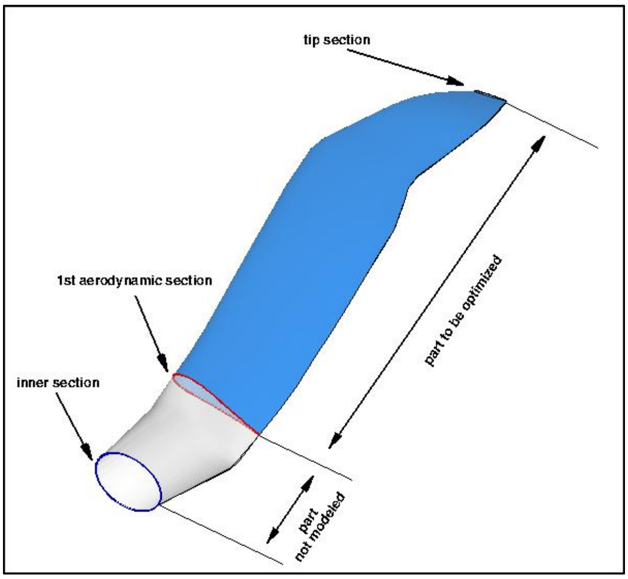

Figure 10: 3D view of the ADYN blade.

Past experiences on helicopter rotors and aircraft propellers have shown that the internal part of the blade close to the hub (cuff), when optimized in the presence of the whole aircraft geometry, can be almost superimposed to the separate optimization of the aerodynamic part of the blade (where cross sections are aerodynamic aerofoils).[14],[8] This simplification reduces the simulation complexity and a satisfactory number of design variables can thus be considered adequate for blade shape optimization. Furthermore, considering that a significant number of simulations are needed both for the exploration of the domain space and the optimization task, the blade is assumed to be rigid which, combined with the simulation of axial flight conditions (hover and cruise at zero incidence), simplifies the rotor trim phase. All of the rotor aerodynamic analyses are performed by trimming the collective pitch to obtain the required nominal thrust.

With respect to the full parametric model described in §3.2, up to 13 of the 20 design variables are simultaneously used here. The following variables are frozen: the vertical and horizontal leading edge position of the three control sections and the twist at the first control section.

Aerofoil	t/c	$C_{l\,max}$	C_d @ C_l=0	M_{dd} @ C_l=0
A1	0.35	1.14 (M=0.3)	0.016 (M=0.3)	0.60
A2	0.20	1.84 (M=0.3)	0.00825 (M=0.4)	0.70
A3	0.12	1.52 (M=0.3)	0.00795 (M=0.6)	0.79
A4	0.09	1.35 (M=0.3)	0.00741 (M=0.6)	0.83
A5	0.07	1.24 (M=0.3)	0.00727 (M=0.6)	0.86

Table 1: aerofoil performance of set A.

Aerofoil	t/c	$C_{l\,max}$	C_d @ C_l=0	M_{dd} @ C_l=0
B1	0.38	1.21 (M=0.3)	0.038 (M=0.3)	0.60
B2	0.20	1.32 (M=0.4)	0.012 (M=0.4)	0.75
B3	0.12	1.50 (M=0.4)	0.0085 (M=0.6)	0.80
B4	0.09	1.24 (M=0.4)	0.0079 (M=0.6)	0.85
B5	0.07	1.21 (M=0.4)	0.00718 (M=0.7)	0.90

Table 2: Aerofoil performance of set B.

5.2. Validation of the numerical procedure

Hereafter a brief validation of the MDA procedure based on the BEMT code is presented with reference to tiltrotor configurations. Figure 11 includes the comparisons on the rotor performance of numerical predictions against the experimental data of the ADYN test campaign.

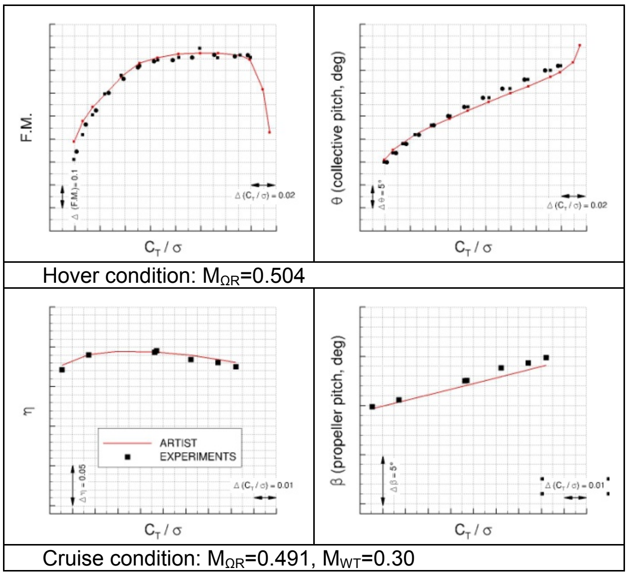

Figure 11: validation of the BEMT code on the ADYN rotor.

The rotational tip velocity is $M_{\Omega R}$=0.504 in hover and $M_{\Omega R}$=0.491 in cruise; the Wind Tunnel flow velocity is M_{WT}=0 in hover and M_{WT}=0.30 in cruise. The ARTIST results shown in this figure comes from the postdictive phase when the code was trained with the help of experimental and CFD data. The use of the coupling procedure where the ARTIST aerodynamics is replaced by CFD aerodynamics has demonstrated to be effective in the predictive phase.

6. RESULTS

The numerical results presented here are relative to rotors which have a constant radius (helicopter and aircraft mode) or a variable rotor radius (helicopter mode).

The investigations aim at exploring the design space and at optimizing the blade shape with specific reference to the aerofoil related design variables. The exploration of the design space is mainly done by means of DOE (Design Of Experiments) evaluations. Multi-Objective Optimization (MOO) is accomplished by using direct simulations. The optimization exercises involve both gradient-based and evolutionary algorithms. The use of a typical gradient based method, NLPQL (Non-Linear Programming by Quadratic Lagrangian) confirms that this method is fast in the optimum search but it is prone to local optimum. It was found that NLPQL is less computational expensive since few evaluations are required to obtain the optima. On the contrary, the use of the evolutionary algorithm NSEA (Non-Dominated Sorting Evolutionary Algorithm) is extremely expensive with respect to the gradient based algorithm.

Pareto fronts are available from MOOs and, in absence of any decision making criterion, designs have been extracted by giving priorities to the optima with equal gains on both objectives and by discarding extreme geometries after a visual inspection.

6.1. Rotors with frozen radius

The first subcase can be synthesized as follows: starting from the existing ADYN blade planform, to find the optimum distribution of the aerofoils adopting the initial blade segments length (equi-spaced segments). The blades are constructed by adopting the same planform data and, alternatively, the two sets of aerofoil data. Because of an equal number of distinct aerofoils for the two sets, the same number of blades with different aerofoils have been generated.

The two level optimization process is arranged so that the optimization on the aerofoil distribution is performed in the outer level and the single evaluation at the nominal conditions in the inner level. Figures 12 and 13 contain the results for the aerofoil set A and B, respectively.

The performance gains, even still significant, are more relevant for set B. Indeed, aerofoil set A was used when the baseline blade was designed. In both figures the designs showing the highest Figure of Merit (FM) and the highest propeller efficiency (η) with limited penalty on FM are emphasized with the diamond and triangle symbols respectively; later they will be called, accordingly, diamond and triangle designs. The corresponding aerofoil distributions can be extracted from Figure 14 where the colours blue and red refer to set A and set B. The relevant difference in aerodynamic performance between the first two aerofoils of each set (A1 vs B1 and A2 vs B2) motivates the inner aerofoil distributions.

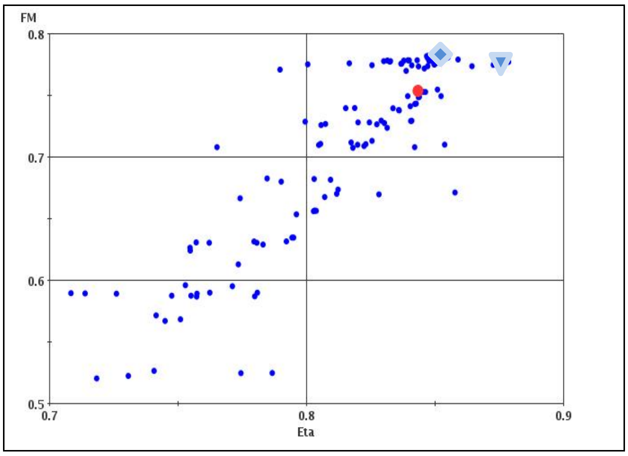

Figure 12: blade designs adopting aerofoil set A in the objective function space (red bullet represents the baseline blade).

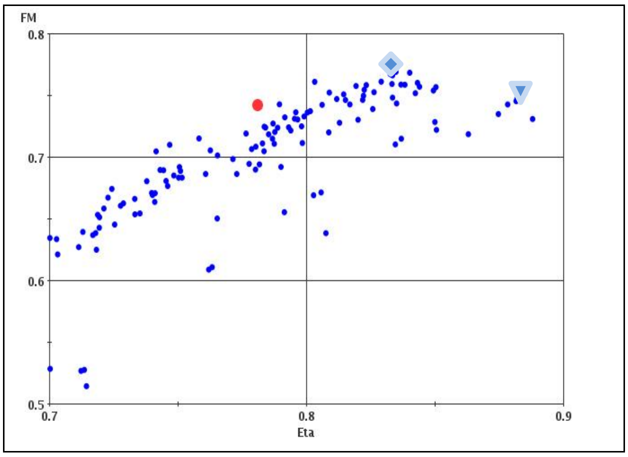

Figure 13: blade designs adopting aerofoil set B in the objective function space (red bullet represents the baseline blade).

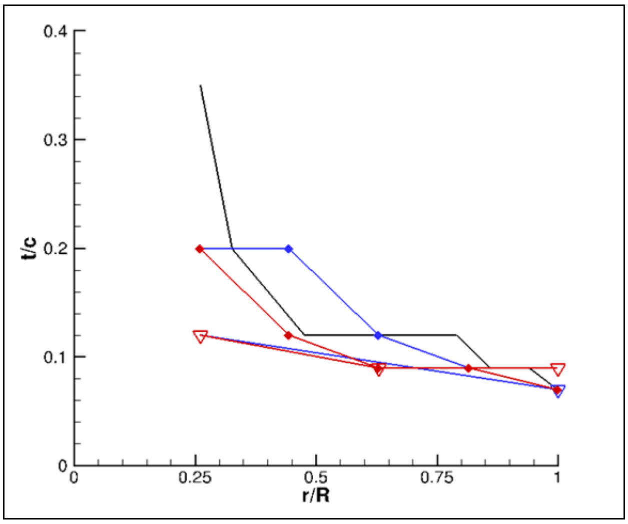

Figure 14: aerofoil distribution. Black line=baseline blade. Blue line=blade with set A. Red line=blade with set B. Symbols refer to diamond and triangle designs.

Anyway, the new distributions allow for substantial rotor performance improvements with respect to the performance of the baseline blade. Furthermore, the gap between the performance of the blades with the two sets of aerofoils is much more reduced both for diamond and triangle designs. Set A of aerofoils allows for better rotor performance in helicopter mode; on the contrary, set B is more promising for rotors in airplane mode.

In the second subcase the design space is extended so that the length of the blade segments is considered as well as. Results in Figures 15 and 16 are reasonably close to those of Figures 12 and 13. The spanwise distribution of the aerofoils is depicted in Figure 17 where it can be observed that high propulsive efficiency for aerofoils set B (triangle design) is obtained thinning almost the whole blade from *t/c*=0.2 to *t/c*=0.07.

The first two subcases try to accommodate the aerofoil distribution to the frozen planform and in particular to the twist law. The assumption on which the investigations are based is that there is a correspondence between the linear variation of the aerofoil geometries and the interpolated aerodynamic look-up tables characteristics.

In order to explore the influence of the rotor radius, the twist law and the rotor angular velocity on the objective functions, the following third subcase has been performed: by maintaining constant the aerofoil distribution coming from the diamond designs of the second subcase, the two level process sees a DOE on the upper level including the variation of the rotor radius and the twist law (which are in common for both tiltrotor operating conditions) and the optimization of the angular velocity with a gradient algorithm on the inner level. This process allows to explore those designs with the same aerofoil distribution and a rotor radius and twist law different from the reference ones at the optimum rotor angular velocity.

Figures 18 and 19 emphasize that new improvements are still possible. As a consequence, the two level process of the third subcase has been rerun after replacing the DOE with a MOO where an evolutionary algorithm (NSEA+) is applied on the upper level of the global optimization process (see Figures 20 and 21).

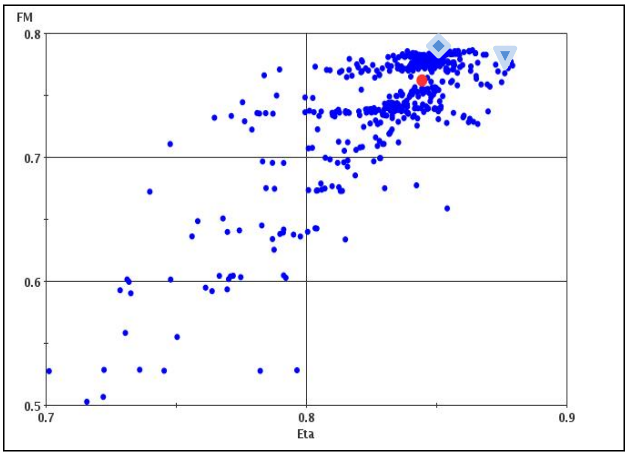

Figure 15: blade designs adopting aerofoil set A in the objective function space (red bullet represents the baseline blade).

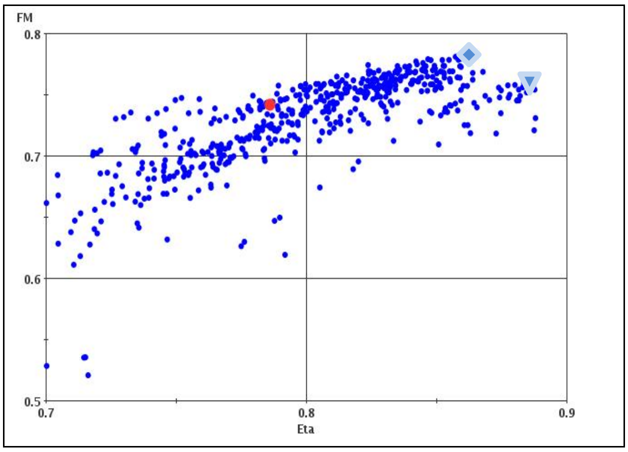

Figure 16: blade designs adopting aerofoil set B in the objective function space (red bullet represents the baseline blade).

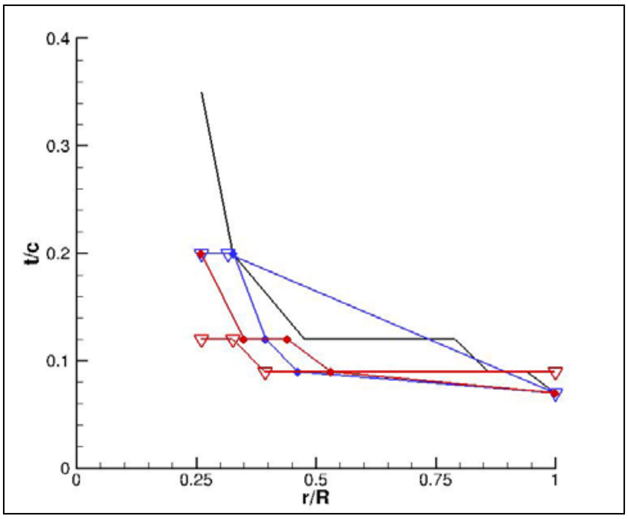

Figure 17: aerofoil distribution. Black line=baseline blade. Blue line=blade with set A. Red line=blade with set B. Symbols refer to diamond and triangle designs.

Table 3 summarizes the results of the third exercise with respect to the baseline blade in terms of percentage increment/decrement of the rotor radius (ΔR), increment of the built-in twist angle at two radial stations (ΔTw1, ΔTw2), the optimum angular velocity in helicopter (ΔRPM_H) and airplane (ΔRPM_A) mode and the ratio between these two velocities ($\Delta RPM_{A/H}$).

There is a general tendency in reducing the radius and the angular velocity in airplane mode and in increasing the twist angles near the blade tip with respect to the baseline values. The ratio of angular velocities in airplane/helicopter mode is greater than that of the baseline rotor. Figure 22 compares the baseline blade with the MOO set A blade of Table 3.

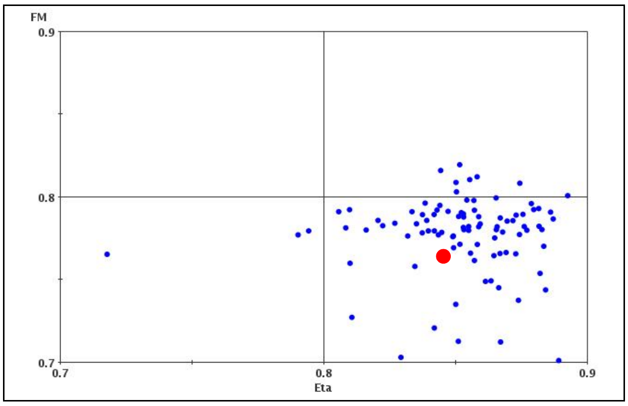

Figure 18: DOE results relative to the diamond design of Figure 15 (set A) by varying rotor radius and twist law at optimum angular velocity.

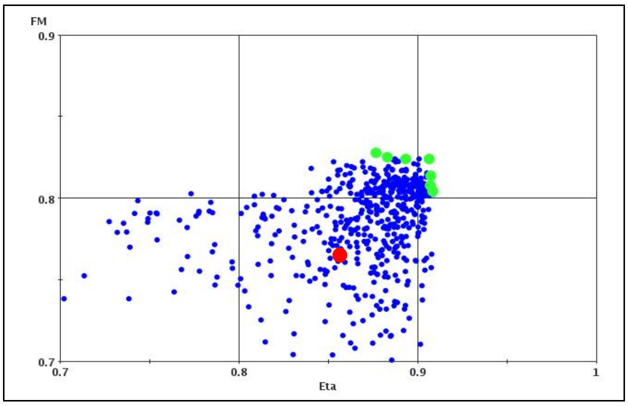

Figure 20: MOO results relative to the diamond design of Figure 15 (set A) by optimizing simultaneously rotor radius and twist law at optimum angular velocity. Green bullets delimit the Pareto front.

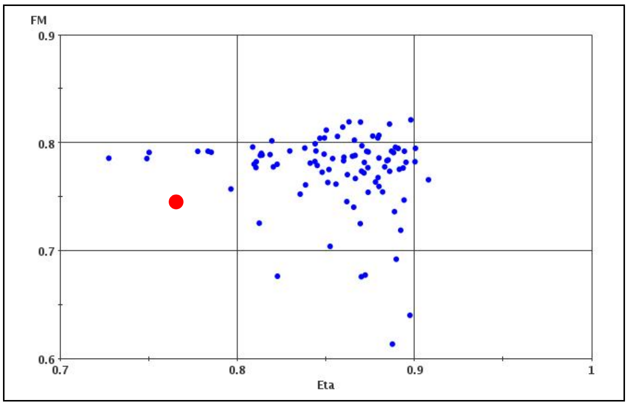

Figure 19: DOE results relative to the diamond design of Figure 16 (set B) by varying rotor radius and twist law at optimum angular velocity.

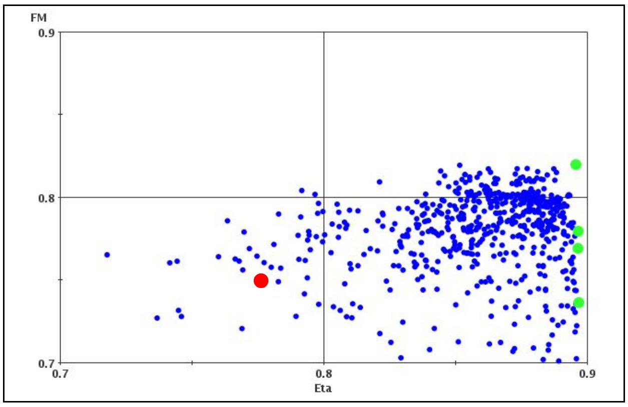

Figure 21: MOO results relative to the diamond design of Figure 16 (set B) by optimizing simultaneously rotor radius and twist law at optimum angular velocity. Green bullets delimit the Pareto front.

	DOE set A	MOO set A	DOE set B	MOO set B
FM	0.821	0.824	0.801	0.819
η	0.898	0.907	0.893	0.896
ΔR	-5.0%	-4.9%	-5.2%	-4.4%
ΔTw1	+1.6° *(r/R=0.7)*	+3.7° *(r/R=0.7)*	+3.12° *(r/R=0.8)*	+3.8° *(r/R=0.6)*
ΔTw2	+3.3° *(r/R=1.0)*	+2.75° *(r/R=1.0)*	+1.05° *(r/R=1.0)*	+2.9° *(r/R=1.0)*
ΔRPM_H	+0.7%	-0.5%	-0.1%	-0.7%
ΔRPM_A	-23%	-20%	-16%	-21%
$\Delta RPM_{A/H}$	-22%	-19%	-17%	-22%

Table 3: summary of the results of the third exercise.

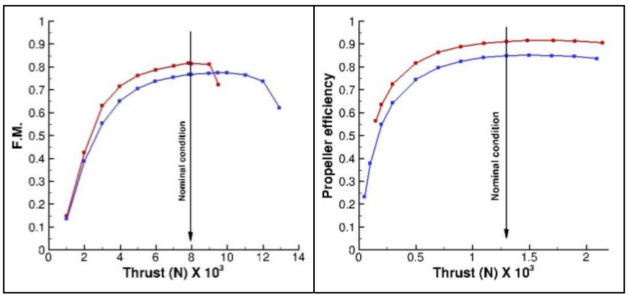

Figure 22: effects of the aerofoil selection and distribution on rotor aerodynamic performance. Red line=MOO set A blade of Table 3; blue line=baseline blade

6.2. Variable diameter rotors

Among the concepts developed over the past years, in this section the concept based on the rigid radial movement of the whole aerodynamic part of the blade is investigated. So, the fourth subcase concerns with the search for that optimum blade which gives the highest propulsive efficiency in cruise and, when elongated, the best figure of merit in hover.

The two level process is articulated as follows: the upper level concerns with the optimization of aerofoil distribution, length of the blade segments and twist law; the inner level is split into two optimizations being the first one relative to the angular velocity and the radius extension in helicopter mode and the second one to the angular velocity of the airplane mode. Originally, in the upper level the rotor radius was included too as design variable. This choice turned to be inconvenient since the upper level dominated on the inner level so that the best designs had almost zero radius extension and a blade configuration very close to that one of the third subcase. The other alternative consisting in letting the two inner optimizations find the optimum rotor length for hover and cruise conditions suffers from the following drawback: the blade segments are proportional to the rotor radius and the selected aerofoils would not be in the same spanwise positions if the radius is different.

Since the third subcase indicates that the optimum radius is slightly shorter than the nominal one, the radius for the fourth subcase is fixed to 85% of the nominal value and it is explored the tip extension up to 40% R. Also the spanwise chord distribution varies.

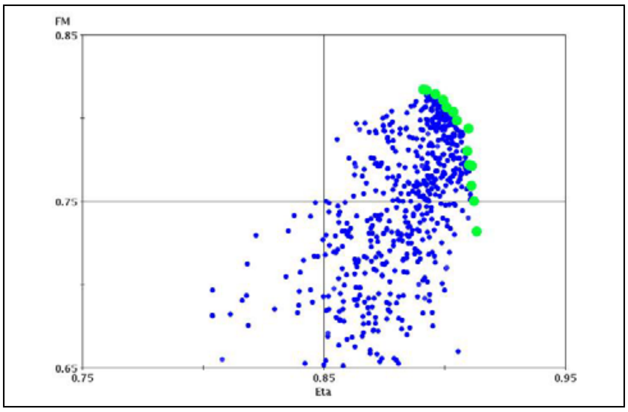

Figure 23: optimization relative to the radial extension of the blade.

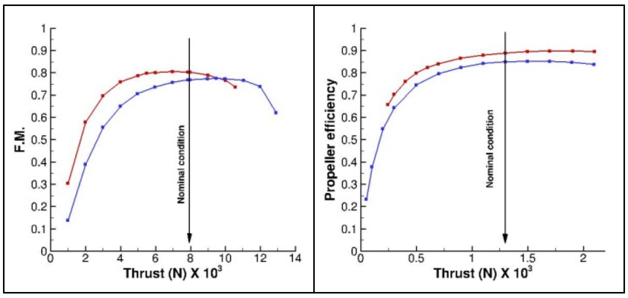

Figure 24: effects of the aerofoil selection and distribution on rotor aerodynamic performance. Red line=blade radially extended; blue line=baseline blade.

Figure 23, which is relative to aerofoil set A, shows encouraging results but the rotor performance is not very far from that obtained for an un-morphed blade. The radial position of the tip is close, when extended to meet the helicopter mode requirements, to the tip of the optimum un-morphed blade (subcase 3). Figure 24 shows that the performance gains are more significant for the airplane mode as expected.

7. OUTLOOK

The optimization of tiltrotor blades is very fascinating and the activities presented in this study are not exhaustive. The choice of the appropriate optimization strategy and algorithm together with the most convenient analysis tools deserves further investigations. The effect of the adoption of more advanced analysis codes will be studied and the greater fidelity will be evaluated against the increased simulation complexity and computational effort.

The next step in this respect will be the embedding within the optimization process of MDA procedures based on CFD codes and, in particular, on Euler-Boundary Layer predictions which will be subsequently coupled to a commercial CSD software (e.g., FLIGHTLAB).

As far as the extension to further investigations, the telescopic blade concept, herein not investigated because of the complexity of the baseline blade tip geometry, will be explored on more conventional blade planforms. A blade concept implementing a variable chord device or an on-off static variable twist will also be considered.

Finally, the analysis of other flight conditions (e.g., descent flight) and off-design points will enrich the definition of the optimization objectives.

8. CONCLUSIONS

A methodology for the aerodynamic shape optimization of tiltrotor blades has been illustrated. It is based on an MDA procedure, implementing a BEMT method, embedded within a commercial optimization environment. The validation has revealed that the BEMT analysis module was able to catch the rotor performance behaviour (FM and η trends versus rotor load).

The potential of this tool has been discussed after performing both design space explorations or optimization tasks. The nature of the applications presented is essentially exploratory since they do not prelude to an industrial project but they are intended to assess the methodology in light of forthcoming research projects. Nevertheless, a blade surface parameterization requiring twenty design parameters, the testing of different optimization techniques, the involvement of both gradient-based and evolutionary algorithms produced a sufficient amount of results to discuss the critical issues that the actual approach presents.

The influence of the aerofoils (in terms of shape and spanwise position) has been emphasized and their optimum selection may lead to significant aerodynamic performance improvements. Of course, the design of advanced aerofoils allows for better sectional aerodynamic performance which is a basic element to further improve the rotor blades.

An optimization on a large number of design variables appears still expensive if performed by using high-order methods because of the number of numerical analyses. Since all of the selected design variables affect the optimization objectives and mutually influence each other, it can be observed that more suitable explorations of the design space requiring the evaluation of thousands (millions, in some cases) of designs makes unaffordable the whole activity. Eventually a new generation of comprehensive rotor codes and Navier-Stokes solvers will be used for optimization too. For the time being, the gradual assessment of less expensive methods provides numerical solutions that can be successfully applied for problems with highly intensive computation requirements.

ACKNOWLEGMENTS

The initial blade geometries and the corresponding aerodynamic data were taken from the documentation of the ADYN project (2002-2007) partially funded by the European Commission under the 5th Framework Programme.

REFERENCES

[1] E. Romander, "3-D Navier-Stokes Analysis of Blade Root Aerodynamics for a Tiltrotor Aircraft in Cruise," Proceeding of the AHS Vertical Lift Aircraft Design Conference, San Francisco, CA, (2006).

[2] C.W. Acree, "Performance Optimization of the NASA Large Civil Tiltrotor," *Proceeding of the International Powered Lift Conference,* London, UK, (2008).

[3] C. Stahlhut and J.G. Leishman, "Aerodynamic Design Optimization of Proprotors for Convertible-Rotor Concepts," *Proceedings of the 68th AHS annual forum.* Fort Worth, TX, (2012).

[4] A. Pagano, "Advanced Tiltrotor Blade Shapes by Multi-Objective Optimization," *Proceedings of Eurogen 2011 Conference,* Capua (CE), Italy, (2011).

[5] www.noesissolutions.com

[6] A. Pagano, "Code Networking for Multi-disciplinary Analysis of Rotor Phenomena," *Air & Space Europe*, Vol. 3, N. 3-4, pp 155-160, Edition Elsevier, (2001).

[7] A. Pagano, L. Federico and L. Notarnicola, "Process Capturing and Optimization for Rotorcraft Systems," *CIRA-TR-07-0152 and*

OPTIMUS Worldwide User Meeting, Leuven, Belgium, (2007).

[8] A. Pagano, M. Barbarino, D. Casalino and L. Federico, "Tonal and Broadband Noise Calculations for Aeroacoustic Optimization of Propeller Blades in a Pusher Configuration," *Journal of Aircraft*, Volume 47, Number 3, (2010).

[9] A. Pagano, S. Ameduri, V. Cokonaj, A. Prachař, Z. Zachariadis and D. Drikakis "Helicopter Blade Twist Control Through SMA Technology: Optimal Shape Prediction, Twist Actuator Realisation and Main Rotor Enhanced Performance Computation," *Proceedings of 35th European Rotorcraft Forum*, Hamburg, Germany, (2009).

[10] B.G. van der Wall and O. Schneider, "Wind Tunnel Tests in DNW: Report of Data acquired by DLR Inst. Of Flight Systems," ADYN consortium confidential report ADYN/WP3/DLR/TR-10/A, (2006).

[11] F. Nannoni, G. Giancamilli and M. Cicalé, "ERICA: the European Advanced Tiltrotor," Proceedings of 27th European Rotorcraft Forum, Moscow, Russia, (2001).

[12] E. Bianchi and P. Beaumier, "Final Optimised Blade Design, Characteristics and Loads," ADYN consortium confidential report ADYN/WP3/AG/D3-7/C, (2003).

[13] T. Lefebvre, P. Beaumier, S. Canard, A. Pisoni, A. Pagano, A. Sorrentino, B. van der Wall, A. D'Alascio, C. Arzoumanian, S. Voutsinas and C. Hermans, "Aerodynamic and Aeroacoustic Optimization of Modern Tilt-Rotor Blades within the ADYN Project," *ECCOMAS-2004 conference*, Jyvaskyla, Finland, (2004).

[14] P. Beaumier, J. Decours and T. Lefebvre, "Aerodynamic and Aero-Acoustic Design of Modern Tilt-Rotors: The ONERA Experience," *26th Congress of International Council of the Aeronautical Sciences (ICAS)* 14 - 19 September 2008, Anchorage, Alaska, USA, (2008).

[15] J. Decours, S. Burguburu and F. Falissard, "Performance Assessment of the Erica Tilt-Rotor in Cruise," 36th European Rotorcraft Forum, Paris, France, (2010).

[16] A. Eberhard and C. Salbashian, "NICETRIP rotor: an optimized tilt-rotor," Proceedings of 69th AHS Annual Forum, Phoenix, Arizona, (2013).